

Structure of gold nanoparticles suspended in water studied by x-ray diffraction and computer simulations

Valeri Petkov,^{1,*} Yong Peng,¹ Geoff Williams,² Baohua Huang,^{3,*} Donald Tomalia,³ and Yang Ren⁴

¹*Department of Physics, Central Michigan University, Mt. Pleasant, Michigan 48859, USA*

²*Department of Biology, Central Michigan University, Mt. Pleasant, Michigan 48859, USA*

³*Dendritic NanoTechnologies, Mt. Pleasant, Michigan 48858, USA*

⁴*Advanced Photon Source, Argonne National Laboratory, Argonne, Illinois 60439, USA*

(Received 20 June 2005; revised manuscript received 22 August 2005; published 3 November 2005)

Gold nanoparticles with an average size of 3 nm, 15 nm, and 30 nm suspended in water have been studied by x-ray diffraction and computer simulations. The atomic pair distribution function approach was employed to determine the three-dimensional structure because of the limited structural coherence in these nanostructured materials. The nanoparticles possess a well-defined atomic arrangement resembling the face-centered cubic (fcc) structure occurring with bulk gold. The fcc-type features of this arrangement become more prominent with increasing nanoparticle size. The study provides a clear picture of the nanoparticles' size-structure relationship and can help open up the route for calculating and predicting of their useful properties.

DOI: [10.1103/PhysRevB.72.195402](https://doi.org/10.1103/PhysRevB.72.195402)

PACS number(s): 61.46.+w, 61.10.Nz, 61.43.Bn

I. INTRODUCTION

In recent years, metallic nanoparticles have attracted much attention because of their unique properties and a wide variety of potential applications. A prime example is gold nanoparticles which are being investigated for applications in selective biological detection,¹ optoelectronics,² and drug delivery.³ It is well known that a material's properties arise from collective atomic effects that are very sensitive to the atomic ordering, including the presence of local structural disorder.⁴ For example, the atomic disorder in gold nanosize structures is seen as broadening in the electron density of states that leads to distinct optical responses for nanoparticles of different sizes and local structures.⁵ Since gold nanoparticles are intensively studied because of their useful properties, a detailed knowledge of their structure, including its imperfections, is needed. However, theoretical studies of the physical properties of gold nanoparticles are hindered by the lack of such knowledge and easy-to-use structural models. The difficulty stems from the fact that materials constructed at the nanoscale level show diffraction patterns with a pronounced diffuse component and a few broad, Bragg-like features. This renders the traditional techniques for structure characterization that are designed to handle either sharp Bragg peaks, to determine the average, longer-range structure, or diffuse scattering alone, to access the local structural imperfections, not quite applicable. Recently, it has been shown that the three-dimensional (3D) structure of materials with reduced structural coherence, including nanocrystalline materials, can be determined in great detail using the atomic pair distribution function (PDF) technique.⁶⁻⁹ Here we use it to determine the 3D structure of dendrimer stabilized gold nanoparticles in water. Nanoparticles with an average size of 3 nm, 15 nm, and 30 nm were studied. The experimental PDFs clearly show that the nanoparticles possess a well-defined atomic arrangement resembling the face-centered cubic (fcc) structure occurring in bulk gold. Also, they show

that the fcc-type arrangement becomes more prominent with increasing nanoparticle size. We find that models based on a fragment of a locally disordered fcc-type structure describe quite well the atomic arrangement in 15 nm and 30 nm nanoparticles. The atomic arrangement in 3 nm nanoparticles is best described by a model that takes into account the presence of extended structural defects and domains inside the nanoparticles.

II. EXPERIMENT

A. Sample preparation

Three systems of gold nanoparticles with average sizes of approximately 3 nm, 15 nm, and 30 nm were studied. The aim was to investigate the effect of particle size on the atomic-scale structure. Gold nanoparticles with a size of 3 nm were synthesized using HAuCl₄ as a precursor. A typical procedure involved mixing of 1 mL of a 4% HAuCl₄ solution with 375 μ L of chloroauric acid and 500 μ L of 0.2 M K₂CO₃ in 100 mL of deionized water. The solution was cooled on ice while stirring rigorously. NaBH₄ solution was added to the chloroauric acid/carbonate suspension while continuing stirring. After completion of the sodium borohydrate addition, the reaction mixture was stirred for 5 min. Cystamine core, hydroxyl surface poly(amidoamine) (PAMAM) dendrimers of a second generation were reduced to thiol-functionalized dendrons and the respective aqueous solution was added to the freshly prepared gold colloidal solution to produce the dendronized nanoparticles. The excess dendron reagent was removed using appropriate Sephadex (G50 and 100) columns. Gold nanoparticles with size of 15 nm were synthesized again using HAuCl₄ as a precursor. A typical procedure involved mixing of 5 mL 1% HAuCl₄ with 4 mL of chloroauric acid and 4 mL of 0.1 M K₂CO₃ in 100 mL deionized water, followed by a thorough mixing and cooling on ice. The next step involved adding of 1 mL of 7%

sodium ascorbate and adjusting the volume of the reaction mixture to 400 mL using deionized water. The mixture was then brought to boil until its color turned red. Thus obtained gold colloidal suspension was reduced to dendron-stabilized gold nanoparticles as described above. Gold nanoparticles with size of 30 nm were synthesized as follows: 0.5 mL of 4% HAuCl₄ was added to 200 mL deionized water. The solution was brought to boil and then 3 mL of 1% sodium citrate were added. The resulted mixture was refluxed for 30 min until its color changed from dark blue to red. The resulted gold colloidal suspension was reduced to dendron-stabilized nanoparticles as described above. More details of the preparation procedures can be found elsewhere.^{10,11}

B. TEM experiments

Transmission electron microscopy (TEM) characterization was performed on a Philips CM12 instrument at 120 keV. All samples were sprayed onto an ultrathin carbon film supported by a 3 mm copper grid and measured after water evaporation. TEM images of the three systems of nanoparticles studied are shown in Fig. 1. Nanoparticle size distributions extracted from the TEM images are shown in Fig. 2.

C. Synchrotron radiation scattering experiments

Previous studies^{7,12} have shown that a nanoparticle's immediate environment, in particular solvent molecules that approach closely all atoms at the nanoparticle's surface, may affect the nanoparticle's atomic ordering substantially. This prompted us to measure the three systems of gold nanoparticles in the environment they are produced and most frequently used, i.e., in water. Diffraction experiments were carried out at the beamline 11-ID-C (at the Advanced Photon Source, Argonne National Laboratory) using x-rays of energy 114.496 keV ($\lambda=0.1083$ Å). During the measurements the samples were contained in sealed glass capillaries. Scattered radiation was collected with an intrinsic germanium detector connected to a multichannel analyzer. The experimental diffraction pattern for 3 nm gold nanoparticles in water is shown in Fig. 3(a). The x-ray diffraction (XRD) patterns for water and crystalline bulk gold are also shown for comparison. As can be seen in the figure, water makes a rather substantial contribution to the total experimental diffraction patterns due to its large volume fraction (approx. 85%). The contribution of the gold nanoparticles is seen as a weak oscillation superimposed on a slowly varying background mostly coming from the water solvent [see Fig. 3(a)]. This oscillation, however, shows up as a well-defined diffraction pattern when the background scattering is removed, as can be seen in Fig. 3(b). The diffraction patterns for the other two systems of gold nanoparticles, corrected for water scattering, are presented in Fig. 3(b) as well.

III. RESULTS

As TEM images reveal, the nanoparticles with an average size of 3 nm [Fig. 1(a)] and 15 nm [Fig. 1(b)] are approximately spherical in shape while those with an average size of 30 nm [Fig. 1(c)] appear as well-developed nanocrystallites

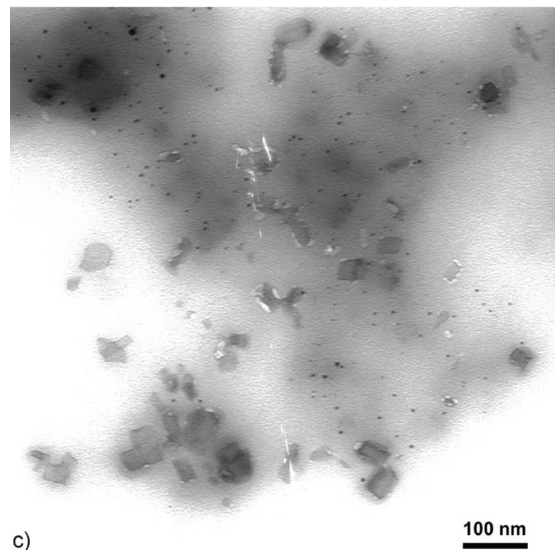
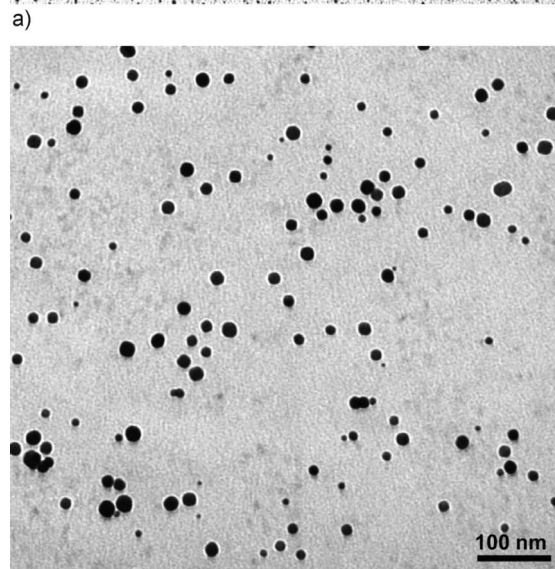
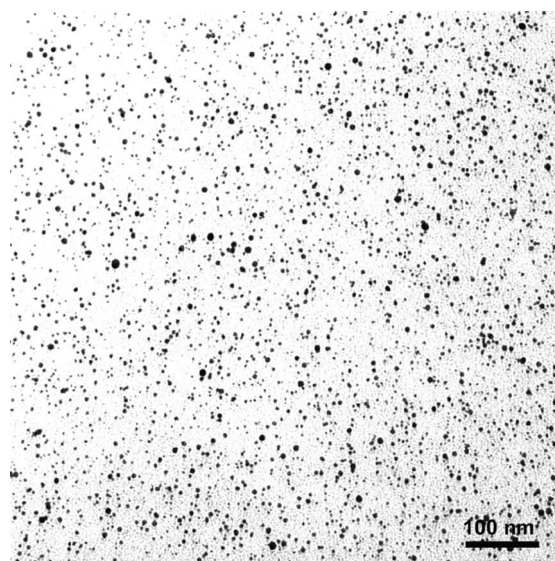


FIG. 1. TEM images of gold nanoparticles with average sizes of 3 nm (a), 15 nm (b), and 30 nm (c).

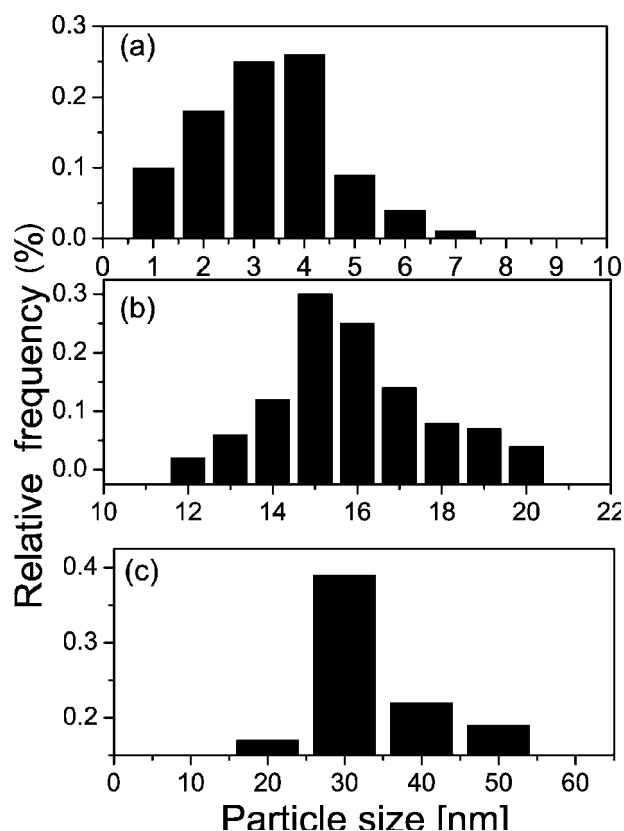


FIG. 2. Distributions of a nanoparticle's size extracted from (a) the TEM image of Fig. 1(a), (b) from the TEM image in Fig. 1(b) and 1(c), from that in Fig. 1(c).

with rectangular shape. Size distributions extracted from the TEM images are relatively narrow (see Fig. 2) with full width at half maximum of approx. 1 nm, 2 nm, and 10 nm for the nanoparticles with an average size of 3, 15, and 30 nm, respectively. The system of 30 nm nanoparticles seems to contain a fraction of smaller nanoparticles, approximately 3–5 nm in size [seen as small dots in Fig. 1(c)]. This fraction, however, constitutes a rather small amount of the sample (~ 1 –2 vol. %) and, since x-ray diffraction is a volume sensitive technique, could hardly affect its x-ray diffraction pattern. As the data in Fig. 3(b) show, the 30 nm crystallites do produce a diffraction pattern that is defined much better than that of the smaller (3 nm system) nanoparticles. As can also be seen in Fig. 1, the nanoparticles in all three samples do not cluster together, likely due to the presence of poly(amidoamine) (PAMAM) dendrons attached to their surface. Obviously the PAMAM dendrons not only stabilize the nanoparticles when suspended in water but prevent them from aggregating when dried in air as well. The PAMAM dendrons attached to the nanoparticle's surface are not visible in the TEM images (see Fig. 1) or in the x-ray diffraction patterns (see Fig. 3) due to the low contrast power of these organic molecules for electrons and x-rays. As previous studies have shown,¹³ the presence of long organic molecules such as PAMAM dendrons does not influence substantially the atomic ordering in the gold nanoparticles they are attached to. The reason is that such chainlike molecules interact with only a few atoms out of a few hundred or thousand

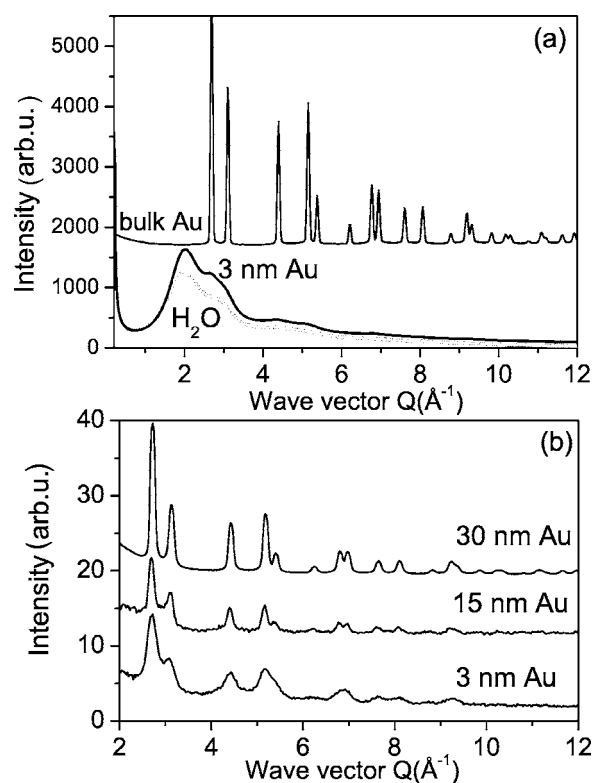


FIG. 3. (a) X-ray diffraction patterns for water (symbols), 3 nm Au nanoparticles in water and bulk gold (solid lines). (b) X-ray diffraction patterns for 3 nm, 15 nm, and 30 nm Au nanoparticles corrected for water and background scattering.

making up the nanoparticles' surface. That is why the presence of PAMAM dendrons was disregarded in the structure analyses carried out by us.

As can be seen in Fig. 3(b) the diffraction patterns for the three systems of gold nanoparticles show several Bragg-like features. Their position and relative intensity match those of the sharp Bragg peaks observed in the diffraction pattern of bulk crystalline gold shown in Fig. 3(a). The Bragg-like features in the diffraction pattern of 3 nm nanoparticles are, however, rather smeared and turn into a slowly oscillating diffuse component at Q values as low as 6 \AA^{-1} . This is due to the truly small particles' size, and, as our subsequent analyses show, to the presence of a considerable local structural disorder. The Bragg-like features in the diffraction patterns of 15 nm and 30 nm are defined better than those in the pattern of the 3 nm nanoparticles but still appear broadened when compared to the corresponding sharp Bragg peaks exhibited by bulk crystalline gold. The analysis of the broadened Bragg-like features in the diffraction patterns of the nanoparticles poses particular problems. Several studies have attempted to interpret them in terms of noncrystallographic clusters¹⁴ or a convoluted mixture of structure types.¹⁵ None of these studies, however, have clearly revealed the effect of particle's size on the atomic-scale structure, nor have they yielded 3D structural models for gold nanoparticles in water in terms of the atomic coordinates. To achieve this goal we considered the diffraction data in terms of the corresponding atomic pair distribution functions. The frequently used atomic pair distribution function $G(r)$ is defined as follows:

$$G(r) = 4\pi r[\rho(r) - \rho_0], \quad (1)$$

where $\rho(r)$ and ρ_0 are the local and average atomic number densities, respectively, and r is the radial distance. It peaks at characteristic distances separating pairs of atoms and thus reflects the atomic-scale structure. The PDF $G(r)$ is the Fourier transform of the experimentally observable structure functions, $S(Q)$, i.e.,

$$G(r) = (2/\pi) \int_{Q=0}^{Q_{\max}} Q[S(Q) - 1] \sin(Qr) dQ, \quad (2)$$

where Q is the magnitude of the wave vector ($Q = 4\pi \sin \theta/\lambda$), 2θ is the angle between the incoming and outgoing radiation beams, and λ is the wavelength of the radiation used. The structure function is related to the coherent part of the total scattered intensity as follows:

$$S(Q) = 1 + [I^{\text{coh}}(Q) - \sum c_i |f_i(Q)|^2] / |\sum c_i f_i(Q)|^2, \quad (3)$$

where $I^{\text{coh}}(Q)$ is the coherent scattering intensity per atom in electron units and c_i and f_i are the atomic concentration and x-ray scattering factor, respectively, for the atomic species of type i . As can be seen from Eqs. (1)–(3), the PDF is simply another representation of the diffraction data. However, exploring the diffraction data in real space is advantageous, especially in the case of materials of limited structural coherence. First, as Eqs. (2) and (3) imply, the *total* scattering, including Bragg peaks as well as diffuse scattering-like features, contributes to the PDF. In this way both the average, longer-range atomic structure, manifested in the Bragg peaks, and the local structural imperfections, manifested in the diffuse component of the diffraction pattern, are reflected in the PDF. And second, the atomic PDFs do not imply any periodicity and can be used to study the atomic ordering in materials showing any degree of structural coherence, ranging from crystals^{6,16} to glasses¹⁷ and even liquids.¹⁸ This is especially important in the present studies where the degree of structural coherence changes across the three different samples of gold nanoparticles studied. Recently the advantages of the atomic PDF approach have been successfully utilized in structure studies of several nanocrystalline materials,^{6–9} including nanoparticles.^{7,19}

Experimental PDFs for the gold nanoparticles and bulk crystalline gold were obtained as follows. First, the coherently scattered intensities were extracted from the XRD patterns shown in Fig. 3 by applying appropriate corrections for flux, Compton scattering, and sample absorption. The intensities were normalized in absolute electron units, reduced to structure functions $Q[S(Q) - 1]$ and Fourier transformed to atomic PDFs. Thus obtained experimental atomic PDFs are shown in Fig. 4. All data processing was done with the help of the program RAD.²⁰

IV. DISCUSSION

As can be seen in Fig. 4(a), the experimental PDF for bulk crystalline gold is rich in well-defined structural features extending to high real-space distances, as it should be with a material possessing a perfect long-range atomic order.

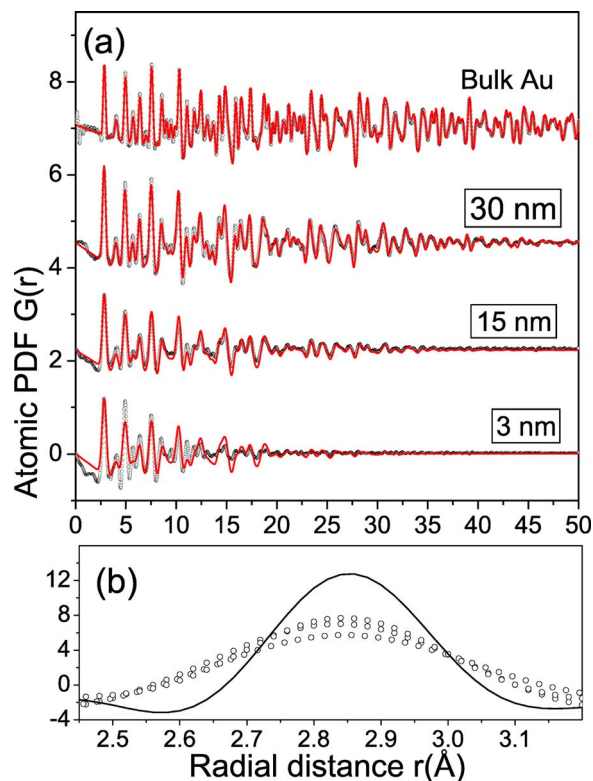


FIG. 4. (Color online) Experimental atomic PDFs (symbols) for gold nanoparticles with an average size of 3 nm, 15 nm, 30 nm, and for bulk gold (a). Model atomic PDFs calculated from structure data for crystalline gold, as described in the text, are shown as solid lines (in red). The first peak in the experimental PDFs for the nanoparticles (symbols) and for bulk gold (solid line) is shown in (b) on an enlarged scale.

The PDFs for the nanoparticles are also rich in structural features but they vanish at much shorter interatomic distances. The nanoparticles, as one may expect, lack the extended order of usual crystals. The first peak in all experimental PDFs is shown in Fig. 4(b). It is positioned at approximately 2.86(2) Å which is the average Au-Au first neighbor distance in gold. A careful inspection of the peak shows that the distribution of Au-Au first neighbor distances in the nanoparticles is considerably broader than that in bulk gold. The broadened distribution of Au-Au first neighbor distances does not scale with the average nanoparticle's size (varying from 3 nm to 30 nm) and, therefore, one may safely assume that it is mostly due to the presence of a considerable local structural disorder in all three systems of nanoparticles studied. Moreover, a closer look at the experimental PDFs for the gold nanoparticles shows that they decay almost to zero at interatomic distances much shorter than the average nanoparticle's size. This observation shows that the local structural disorder and not the particle's size is the factor limiting the structural coherence in the nanostructured gold studied by us.

To assess the details of the atomic-scale structure in the nanoparticles we attempted to approximate their experimental PDFs with a model based on the face-centered cubic structure [see Fig. 5(c)] occurring with crystalline gold. The model calculations were done with the help of the program

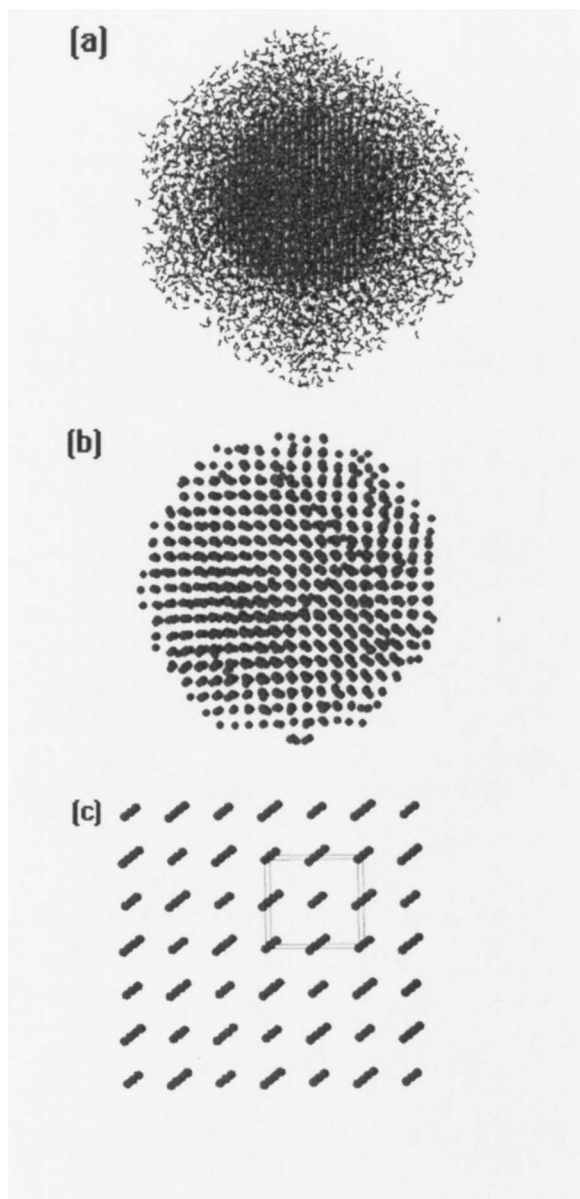


FIG. 5. Computer generated model of a 3 nm gold nanoparticle (circles) in water (short bars) (a). The same nanoparticle is shown in (b) with the water molecules removed for the sake of clarity. The nanoparticle has a moderately relaxed surface and a more densely packed interior divided into domains that are misoriented with respect to each other. A fragment of the fcc lattice of bulk gold is shown in (c) for comparison. The cubic unit cell is outlined with thin solid lines.

PDFFIT.²¹ The program uses crystal structure data such as unit cell constants, atomic coordinates, and thermal factors (mean-square atomic displacements) to compute model PDFs. As can be seen in Fig. 4(a) the experimental data for bulk gold are very well reproduced by the fcc-structure based model. The very good agreement between the model and experiment well documents the fact that the atomic PDFs are a true representation of the atomic ordering in materials and can provide a good quantitative basis for the testing and verifying of structural models. To mimic the presence of local structural disorder in the nanoparticles we artificially en-

larged the mean-square displacements of the atoms in the model atomic configurations from $u_{Au}=0.010 \text{ \AA}^2$ for crystalline gold to $u_{Au}=0.020 \text{ \AA}^2$, $u_{Au}=0.033 \text{ \AA}^2$, and $u_{Au}=0.045 \text{ \AA}^2$ for the 30 nm, 15 nm, and 3 nm nanoparticles, respectively. Furthermore, we multiplied the model PDF data with a decaying exponent as originally suggested by Ergun and Schehl²² and later on implemented in a similar manner by Gilbert *et al.*⁷ As can be seen in Fig. 4(a) the experimental PDFs for the 15 nm and 30 nm nanoparticles can be approximated very well by such a locally disordered fcc-type structure. The agreement between the model and experimental data for the 3 nm nanoparticles is not as good but still acceptable given the high degree of structural disorder present in the material. The result clearly shows that the atomic ordering in bulk and nanostructured gold studied by us is of the same type but differs in its perfection in the different samples. Also, it shows that the atomic ordering in 3 nm nanoparticles departs from the face-centered cubic one in a substantial way and may not be fully accounted for by a fragment of locally disordered fcc lattice alone.

To obtain a more realistic model for the 3D structure of 3 nm gold nanoparticles we employed potential-based computer simulations and verified their outcome against the experimental PDF data. We adopted Monte Carlo simulations because the size of the 3 nm nanoparticle prevented the use of more precise *ab initio* simulation techniques. The simulations were based on an effective pairwise potential for gold that satisfies the bulk cohesive energy and the bulk stability condition exactly.²³ Furthermore, the potential employs additional adjustable parameters that scale with the size of the model system and indirectly take into account the many-body contributions to the potential energy. The potential was tested by successfully simulating the fcc structure of bulk gold starting from a random atomic configuration subject to periodic boundary conditions. The interaction between the water molecules was modeled using a TIP4P-type potential²⁴ and that between gold and water was approximated with a Lennard-Jones type potential ignoring the adsorption of water molecules.²⁵ The simulations were done with the help of the computer program BOSS.²⁶ They were performed on a model nanoparticle of 2000 gold atoms with a size of approximately 3 nm surrounded by 3000 water molecules. Several initial configurations for the gold atoms were tested, including random and completely ordered (fcc-type) ones. The simulations were run long enough both to avoid the possible influence of the initial conditions and to minimize the total energy of the model system. It is well known that a model of given size can visit several local energy minima, each corresponding to a different atomic arrangement. To avoid being trapped in a local minimum we calculated the atomic PDFs for the relaxed atomic configurations and compared them to the experimental PDF for 3 nm nanoparticles. The potential parameters were adjusted until the simulations resulted in a model that is independent on the initial conditions, corresponds to a minimum in the total potential energy, and reproduces the experimental PDF data reasonably well. The approach of using a structure-sensitive experimental quantity to discriminate between competing models is widely applied in traditional crystallography. Here we apply it to find a realistic model for nanosize objects with an imperfect

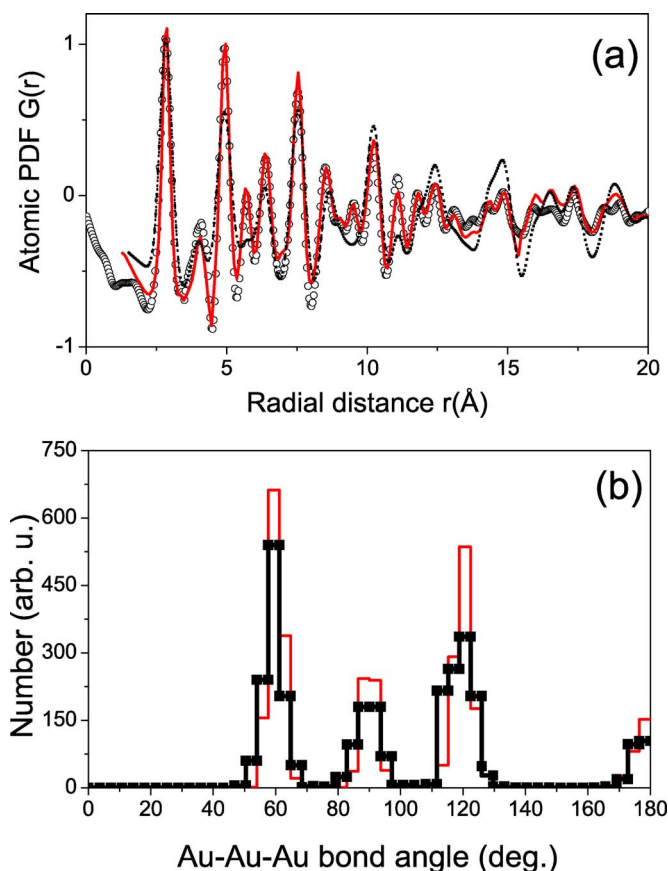


FIG. 6. (Color online) Comparison between the experimental (symbols) and model PDFs for 3 nm gold nanoparticles (a). The model PDFs are calculated from the Monte Carlo generated atomic configuration shown in Fig. 5(b) (solid line in red) and on the basis of a locally disordered fcc-type lattice (broken line in black) as described in the text. Distribution of bond angles in the Monte Carlo generated configuration (symbols) and in bulk crystalline gold (solid line in red) (b).

yet well-defined atomic-scale structure. A typical representative of the model atomic configurations obtained in the manner described above is shown in Fig. 5(a). The corresponding atomic PDFs is compared to the experimental one in Fig. 6(a). The agreement between the calculated and experimental data is better than that achieved with the fcc-lattice type model clearly showing that the potential-based model captures very well the essential structural features of 3 nm gold nanoparticles in water. The model nanoparticle, stripped out of the surrounding water molecules, as shown in Fig. 5(b), is available from the authors upon request. Analysis of the model atomic configuration allows to draw important conclusions about the atomic arrangement in 3 nm gold nanoparticles. The model gold nanoparticle is spherical in shape which is consistent with the TEM observations [see Fig. 1(a)]. The atoms at the particle’s surface are not so densely packed as those in the core of the particle. However, the structural distortion associated with the surface relaxation does not seem to destroy the fcc-type atomic arrangement in the nanoparticle. This is demonstrated by the fact that the distribution of bond angles in the model atomic configuration is only slightly broader than that in the perfect fcc-type lat-

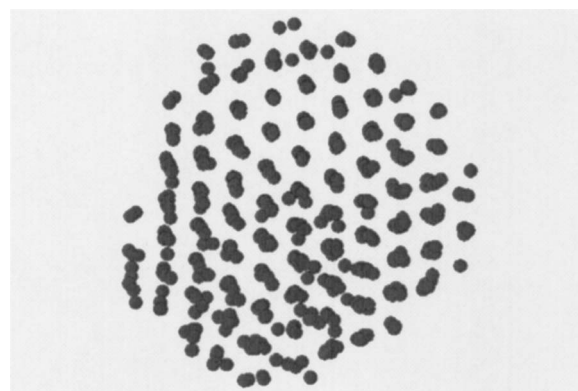


FIG. 7. Computer generated model of a 2 nm gold nanoparticle (circles). Water molecules surrounding the nanoparticle are not shown for the sake of clarity.

tice used to approximate the PDF data for bulk gold [see Fig. 6(b)]. Interestingly, the atomic arrangement in gold nanoparticles we modeled in the absence of water turned out to be less distorted than that observed in nanoparticles modeled in water. This observation is in line with the findings of other independent studies on gold nanoparticles in air.¹⁹ It is, however, in sharp contrast to what has been observed with ZnS nanoparticles which appear to be more ordered in water than in air.¹² A careful inspection of the model presented in Fig. 5(b) also shows that gold nanoparticles as small as 3 nm in size are likely to exhibit extended structural defects, resembling wedge disclinations,²⁷ dividing the inner part of the nanoparticle into regions or domains that are misoriented with respect to each other. The presence of such structural defects in gold nanoparticles of similar size has been confirmed by high resolution TEM (HRTEM) experiments.^{15,19} Furthermore, using the same set of potential parameters we modeled gold nanoparticles of a smaller size (~ 2 nm in diameter) in water. A typical representative of the model atomic configurations for 2 nm nanoparticles is shown in Fig. 7 and is also available from the authors upon request. The atomic arrangement in the 2 nm nanoparticles appeared more imperfect than that in the 3 nm nanoparticles as a comparison between the model configurations presented in Fig. 5(b) and Fig. 7 shows. This finding reinforces our observation [see the experimental PDFs in Fig. 4(a)] that the degree of structural coherence in gold nanoparticles suspended in water scales with their size. Our model results suggest that gold nanoparticles of a size less than 2 nm are even more structurally disordered and their atomic arrangements are likely to exhibit amorphouslike or noncrystallographic (e.g., icosahedral) features. Evidence for such a behavior has been found in other independent studies of gold clusters and nanometer-size particles.^{14,28–30}

V. CONCLUSION

The 3D structure of gold nanoparticles with an average size of 3 nm, 15 nm, and 30 nm in water has been studied by the PDF technique. The nanoparticles have a well-defined atomic arrangement resembling the fcc-type structure occur-

ring in bulk gold. The nanoparticles, however, exhibit a considerable local structural disorder which diminishes with their size. Models based on a fragment of a locally disordered fcc-type lattice provide a very good description of the 3D structure of 15 nm and 30 nm nanoparticles, and, to a good first approximation, that of 3 nm nanoparticles. The atomic arrangement in nanoparticles of size 3 nm and smaller is better described by models that take into account the presence of extended structural defects, domains inside the nanoparticles, and possible noncrystallographic features. The clear understanding of the nanoparticles' size-structure relationship and the practical model considerations resulted from the present study are an important step toward a better understanding of technologically important gold nanoparticles and can help open up the route for calculating and predicting their useful properties.

The results of the present study are a direct demonstration of the ability of the PDF technique to yield three-dimensional structural information for materials of limited structural coherence, including nanoparticles in solution. The

technique succeeds because it relies on total scattering data obtained from the material, and as a result, is sensitive to its essential structural features regardless of crystalline periodicity and size. This allows a convenient testing and refining of structural models. Furthermore, the technique probes the bulk and can provide an important foundation to imaging techniques such as transmission electron and atomic force microscopy, which reveal only structural features projected down one axis or to a surface.

ACKNOWLEDGMENTS

Thanks are due to Mark Beno, Argonne National Laboratory for the help with the synchrotron experiments. This work was supported by the Army Research Laboratory under Cooperative Agreement DAAD19-03-2-0012 and in part by NSF through Grant No. DMR-0304391 (NIRT). The Advanced Photon Source is supported by DOE under Contract No. W-31-109-Eng-38.

*Authors to whom correspondence should be addressed: petkov@phy.cmich.edu, huang@dnanotech.com

¹S. Y. Park and D. Stroud, *Phys. Rev. B* **68**, 224201 (2003); V. Pavlov, Y. Xiao, and I. Willner, *Nano Lett.* **5**, 649 (2005).

²H. Imahori and S. Fukuzumi, *Adv. Mater. (Weinheim, Ger.)* **13**, 1197 (2001); E. Dulkeith, M. Ringler, T. A. Klar, J. Feldman, A. M. Javier, and Parak, *Nano Lett.* **5**, 585 (2005).

³Y. S. Jo, D. K. Kiwi, and M. Muhammed, *J. Mater. Sci.: Mater. Med.* **15**, 1291 (2004); G. F. Paciotti, L. Myer, D. Weinreich, D. Goia, N. Pavel, R. E. McLaughlin, and L. Tamarkin, *Cancer Drug Deliv* **11**, 169 (2004).

⁴L. M. Liz-Marzan and P. Mulvaney, *J. Phys. Chem. B* **107**, 7312 (2003).

⁵I. L. Garzon, E. Artacho, M. R. Beltran, A. Garcia, J. Junquera, K. Michaelian, P. Ordejon, C. Rovira, D. Sanchez-Portal, and J. M. Soler, *Nanotechnology* **12**, 126 (2001); T. G. Schaaff, M. N. Shafiqulin, J. T. Khoury, I. Vezmar, R. L. Whetten, W. G. Cullen, P. N. First, C. Guitierrez-Wing, J. Ascensio, and M. J. Yacaman, *J. Phys. Chem. B* **101**, 7885 (1997); I. L. Garzon, K. Michaelian, M. R. Beltran, A. Posada-Amarillas, P. Ordejon, E. Artacho, D. Sanchez-Portal, and J. M. Soler, *Phys. Rev. Lett.* **81**, 1600 (1998).

⁶W. Dmowski, T. Egami, K. E. Swider-Lyons, C. T. Love, and D. R. Rolison, *J. Phys. Chem. B* **106**, 12677 (2002); V. Petkov, E. Bozin, S. J. L. Billinge, T. Vogt, P. Trikalitis, M. Kanatzidis, *J. Am. Chem. Soc.* **124**, 10157 (2002); V. Petkov, S. J. L. Billinge, T. Vogt, and A. S. Ichimura, *J. L. Dye, Phys. Rev. Lett.* **89**, 075502 (2002); T. Egami and S. J. L. Billinge, *Underneath the Bragg Peaks—Structural Analysis of Complex Materials* (Pergamon Press, Amsterdam, 2003).

⁷B. Gilbert, F. Huang, H. Z. Zhang, G. A. Waychunas, and J. F. Banfield, *Science* **305**, 65 (2004).

⁸V. Petkov, S. J. L. Billinge, P. Larson, S. D. Mahanti, T. Vogt, K. K. Rangan, and M. G. Kanatzidis, *Phys. Rev. B* **65**, 092105 (2002).

⁹V. Petkov, P. Y. Zavalij, S. Lutta, M. S. Whittingham, V. Parvanov, and S. Shastri, *Phys. Rev. B* **69**, 085410 (2004).

¹⁰B. Huang and D. A. Tomalia, *J. Lumin.* **111**, 215 (2005).

¹¹T. Greg, *Bioconjugate Techniques* (Academic Press, San Diego, 1996).

¹²H. Zhang, B. Gilbert, F. Huang, and J. Banfield, *Nature* **424**, 1025 (2003).

¹³K. Yin, Q. Xia, D. Xu, H. Xi, X. Sun, and C. Chen, *Macromol. Theory Simul.* **12**, 593 (2003).

¹⁴C. L. Cleveland, U. Landman, T. G. Schaaff, M. N. Shafiqulin, P. W. Stephens, and R. L. Whetten, *Phys. Rev. Lett.* **79**, 1873 (1997).

¹⁵D. Zanchet, B. D. Hall, and D. Ugarte *J. Phys. Chem. B* **104**, 11013 (2000).

¹⁶V. Petkov, I-K. Jeong, J. S. Chung, M. F. Thorpe, S. Kycia, and S. J. L. Billinge, *Phys. Rev. Lett.* **83**, 4089 (1999).

¹⁷V. Petkov, S. J. L. Billinge, S. D. Shastri, and B. Himmel, *Phys. Rev. Lett.* **85**, 3436 (2000).

¹⁸V. Petkov and G. Yunchov, *J. Phys.: Condens. Matter* **8**, 6145 (1996).

¹⁹K. Page, Th. Proffen, H. Terrones, M. Terrones, L. Lee, Y. Yang, S. Stemmer, R. Seshardi, and A. K. Cheetam, *Chem. Phys. Lett.* **393**, 385 (2004).

²⁰V. Petkov, *J. Appl. Crystallogr.* **22**, 387 (1989).

²¹Th. Proffen and S. J. L. Billinge, *J. Appl. Crystallogr.* **32**, 572 (1999).

²²S. Ergun and R. R. Schehl, *Carbon* **11**, 127 (1973).

²³S. Erkos, *Physica E (Amsterdam)* **8**, 210 (2000).

²⁴W. L. Jorgensen, J. Chandrasekhar, J. D. Madura, R. W. Impey, and M. L. Klein, *J. Chem. Phys.* **79**, 926 (1983).

²⁵S-P. Ju, *J. Chem. Phys.* **122**, 094718 (2005).

²⁶W. L. Jorgensen, D. S. Maxwell, and J. Tirado-Rives, *J. Am. Chem. Soc.* **118**, 11225 (1996); W. L. Jorgensen, *BOSS Version*

- 4.3 (Yale University, New Haven, CT, 2001).
- ²⁷M. Yu. Gutkin and I. A. Ovid'ko, *Rev. Adv. Mater. Sci.* **4**, 79 (2003).
- ²⁸X. Yu and P. M. Duxbury, *Phys. Rev. B* **52**, 2102 (1995).
- ²⁹C. Mottet, G. Treglia, and B. Legrand, *Surf. Sci.* **383**, L719 (1997).
- ³⁰W. Vogel, B. Rosner, and B. Tesche, *J. Phys. Chem.* **97**, 11616 (1993).